Qufei Li, Sherry Wanderling, Pornthep Somponspisut and Eduardo Perozo

Structural Basis of Lipid-Driven Conformational Transitions in the KvAP Voltage Sensing Domain

*To whom correspondence should be addressed. E-mail: eperozo@uchicago.edu

Supplementary Information:

Supplementary Figures 1-5

Supplementary Table 1, 2

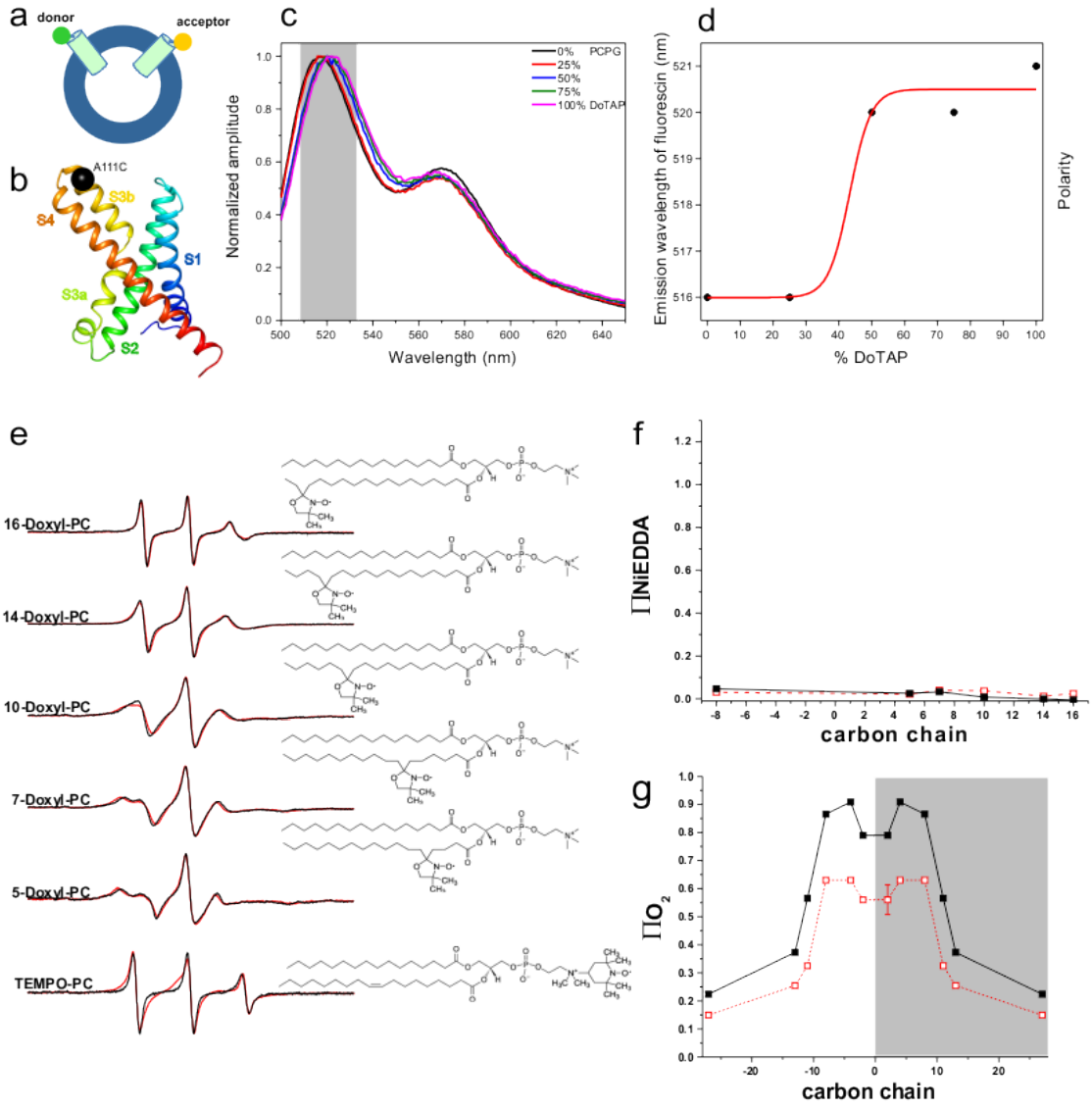
a
donor
acceptor
b
A111C
S3b
S4
S1
S3a
S2
c
0% PCPG
25%
50%
75%
100% DoTAP
Normalized amplitude
Wavelength (nm)
d
Emission wavelength of fluorescin (nm)
Polarity
% DoTAP
e
16-Doxyl-PC
14-Doxyl-PC
10-Doxyl-PC
7-Doxyl-PC
5-Doxyl-PC
TEMPO-PC
f
ΠNiEDDA
carbon chain
g
Πo2
carbon chain

Supplementary Figure 1. Sample characterization: 1. FRET assay indicates no aggregation of KvAP-VSD in both PC:PG and DOTAP liposomes. (**a**) Cartoon representation of FRET assay to evaluate the aggregation behavior. KvAP-VSD mutant A111C (**b**) was individually labeled with fluorescence donor and acceptor, then mixed at 1:1 molar ratio and reconstituted into liposomes. FRET signal in the range of 560-580 nm indicates of closeness of fluorephores in liposome, thus the degree of protein aggregation (see Methods for details). (**c**) Amplitude normalized FRET spectra of KvAP-VSD in liposomes with incremental DOTAP contents. The intensity within region 560-580 nm is essentially the same among all tested conditions, which suggest no severe aggregation of KvAP-VSD in both POPC:POPG and DOTAP liposomes. (**d**) Conformation dependent polarity change upon increment of DOTAP content shown by the wavelength shift of fluorecin emission (grey region, (**c**)). The sigmoidal fit agrees very well with the titration results monitored by spin labeling methods (Fig. 2). 2. DOTAP liposome is physically equivalent to POPC:POPG liposome regarding to oxygen and NiEdda accessibilities. (**e**) EPR spectra of nitroxide radicals at various depths in both PC:PG and DOTAP liposomes, probed by radical containing phosphocholine lipids (see Methods for details). (**f**) No NiEdda accessibility (ΠNi) was observed at all studied positions in both liposomes. (**g**) Oxygen accessibility (ΠO_2) was centralized in the middle of lipid bilayer and decreased toward the surface of liposomes. Both liposomes have the same pattern with slightly different amplitudes.

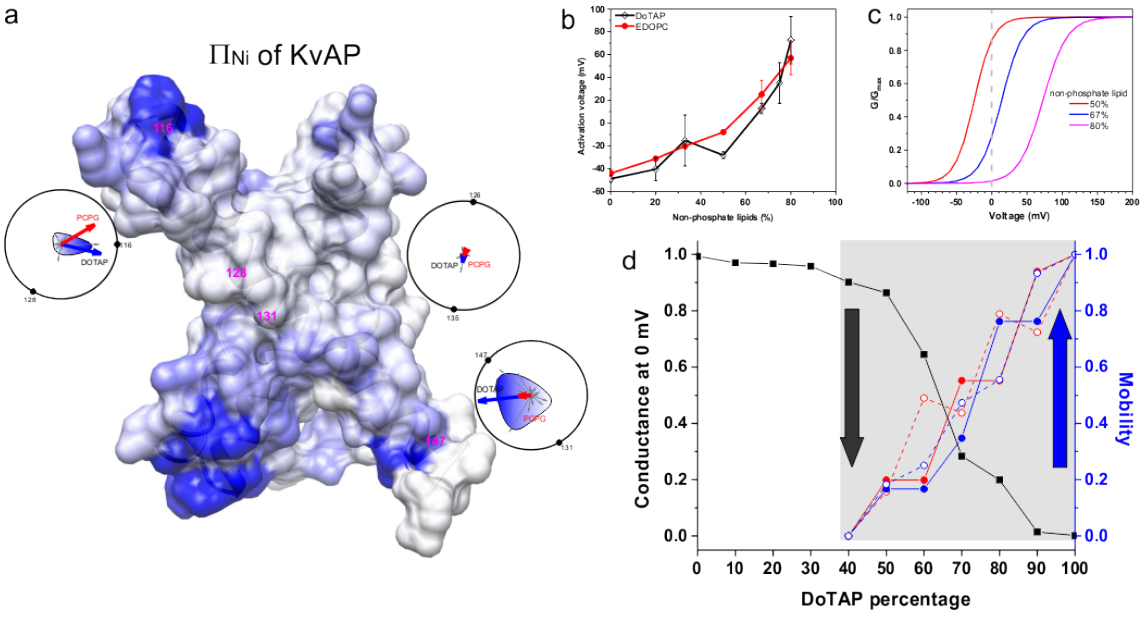

Supplementary Figure 2. Data interpretation. 1. The tilt of S4 from PC:PG to DoTAP shown by the vector presentation ΠNiEdda. ΠNi in DOTAP was mapped onto crystal structure with linear blue scale. There is no water accessibility to the center of membrane. The net difference of ΠNi on extracellular and intracellular ends clearly indicates a tilt trend in the direction opposite to the ΠNi. 2. Coupling of sensor, pore and the ion conduction. KvAP G-V curves (**c**) with different non-phosphate lipid contents (50%, 67% and 80%) were simulated with published V_h (**b**) and z values. At 0 mV, the ion conduction decreases upon DOTAP content increment from 40% to 100% ((**d**) black square), which overlaps exactly with the synchronized mobility increase of both S4 bottom and pore. The coupling of sensor and the pore of the KvAP leads to the functional difference.

a

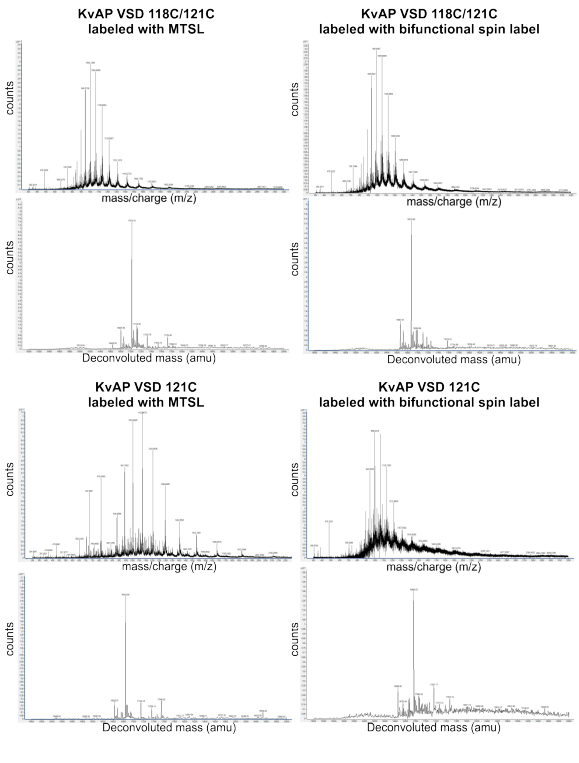

b

Protein	Label	Expected MW (Da)	MS result (Da)	ΔDa	Notes
KvAP VSD 121C	N/A	16656.6	16656.8	0.2	
	MTSL	16842.9	16843.1	0.2	Single MTSL
	Bi-SL	16964.7	16966.5	1.8	Single Bi-SL
KvAP VSD 118C/121C	N/A	16646.6	16646.9	0.0	
	MTSL	16832.9 **17019.2**	17019.2	0.0	Two MTSL
	Bi-SL	16954.7 17262.8 **16874.5**	16874.8	0.3	Single Bi-SL dual attachment

c

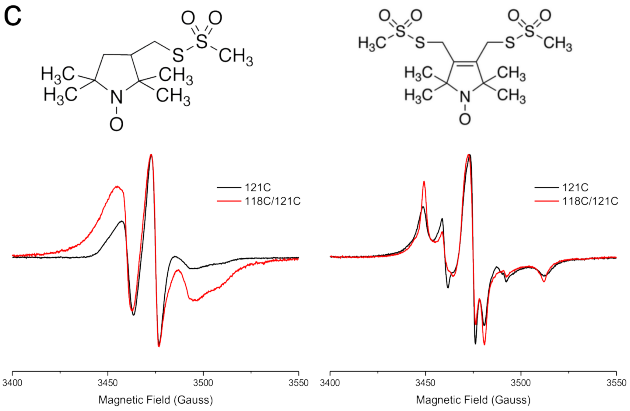

Supplementary Figure 3. Spin labeling efficiency on KvAP VSD cysteine mutant. (**a**) ESI-TOF mass spectrometry analysis for labeled (with either MTSL or bifunctional spin label) KvAP VSD cysteine mutants (either 118C/121C or 121C). The m/z of ionized fragments (top) and deconvoluted mass (bottom) were shown for each of four samples. The spin labeled protein has predominant peak in the MS spectra. (**b**) Summary of the MS results confirming the correct bi-functional attachment of Bi-SL onto the sensor. In particular, there are three possibilities for a bifunctional spin label attaching to double cysteine mutant: 1. Sinlge Bi-SL on one of the cysteine (expected MW, 16954.7); 2. Two Bi-SL on both single cysteine (expected MW, 17262.8); 3. Single Bi-SL on two cysteine (expected MW, 16874.5). The MS unambiguously confirms that both reaction group of Bi-SL were removed through reaction with two cysteine groups. (**c**) Continuous EPR spectra of MTSL labeled (left) and Bi-SL labeled (right) samples. Two MTSL on to adjacent positions shows characteristic dipolar coupling (left, red). At the labeling condition with 20X molar excess of spin label, if a Bi-SL didn't react with both cysteines

together, the double cysteine mutant would be labeled with two Bi-SL which will show significant bipolar coupling feature in CW-EPR spectra.

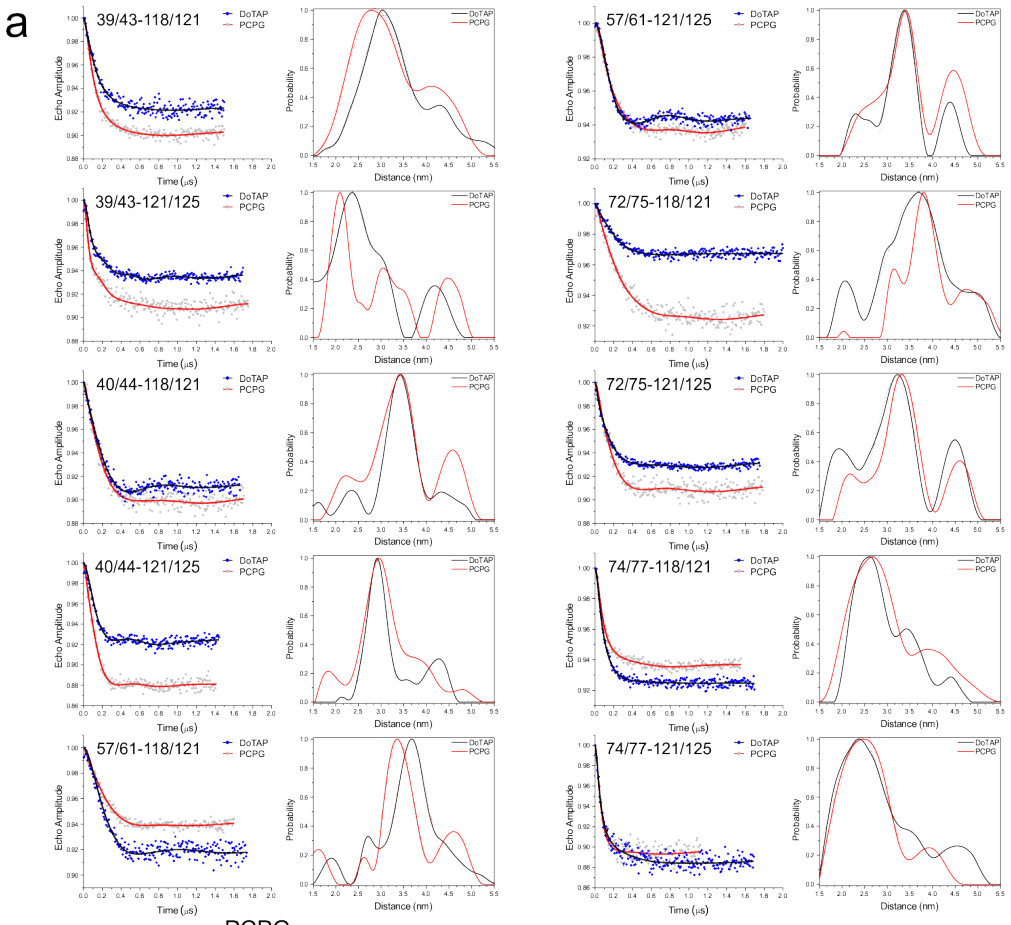
a
39/43-118/121
39/43-121/125
40/44-118/121
40/44-121/125
57/61-118/121
57/61-121/125
72/75-118/121
72/75-121/125
74/77-118/121
74/77-121/125
DoTAP
PCPG
Echo Amplitude
Time (μs)
Probability
Distance (nm)

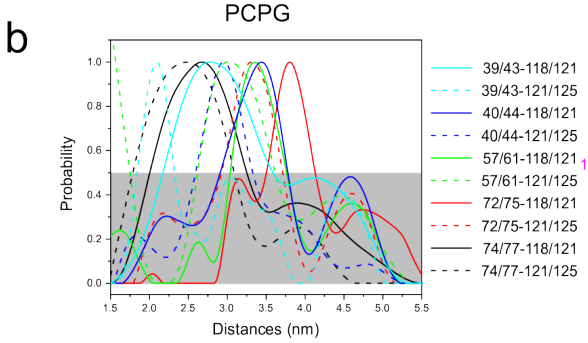
b
PCPG
Probability
Distances (nm)
39/43-118/121
39/43-121/125
40/44-118/121
40/44-121/125
57/61-118/121
57/61-121/125
72/75-118/121
72/75-121/125
74/77-118/121
74/77-121/125

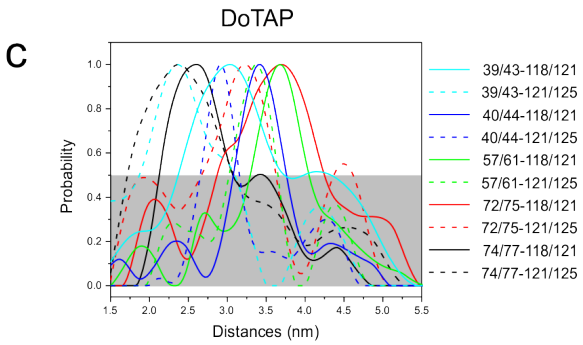
c
DoTAP
Probability
Distances (nm)
39/43-118/121
39/43-121/125
40/44-118/121
40/44-121/125
57/61-118/121
57/61-121/125
72/75-118/121
72/75-121/125
74/77-118/121
74/77-121/125

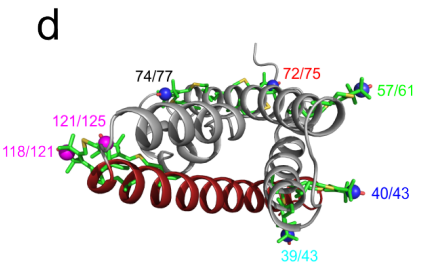
d
74/77
72/75
57/61
121/125
118/121
40/43
39/43

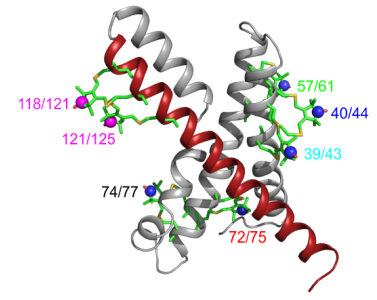
118/121
57/61
40/44
121/125
39/43
74/77
72/75

Supplementary Figure 4. Background corrected echo decay and distance distribution of 10 pairs of DEER measurement in PCPG and DOTAP liposomes (**a**). The dipolar evolution in PCPG (grey circle) and DOTAP (blue circle) were analyzed by Tikhonov regularization. The fit and the resulting distance distribution are shown in red (PCPG) and black (DOTAP) lines. The distances are consistent with geometric patterns indicated by crystal structure. Predominant single main peak (above the grey region) is clearly resolved for all 10 pairs of distances in two liposomes ((**b**) PCPG and (**c**) DOTAP) among the range of 22 to 38 Å, which lay in the most sensitive region of the pulsed EPR method. All 10 distances measured with 118/121 (left, solid line) are larger than the corresponding distances with 121/125 (left, dash line), which are consistent with 118/121 are further than 121/125 to all reference points (**d**). The same consistency was also observed for 40/44 > 39/43 ((**d**), top) and 72/75 > 74/77 ((**d**), bottom) in all measured distances ((**b**) and (**c**)).

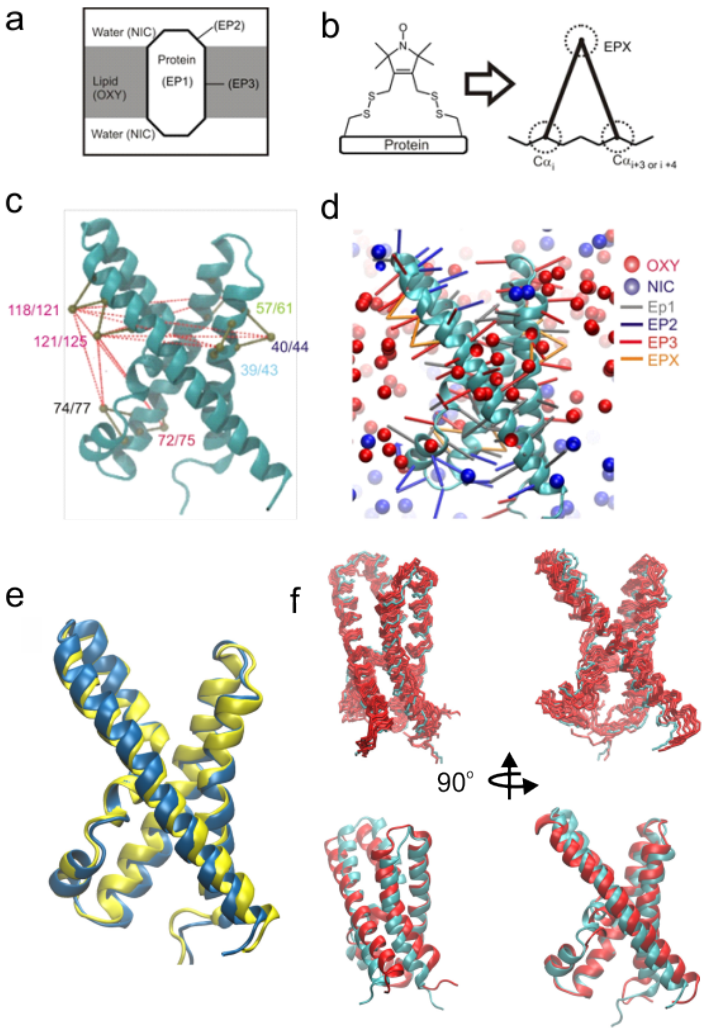

Supplementary Figure 5 General scheme of MD simulation and the structural models. (**a**) Simple representation of the pseudo-spin (EP1, EP2 and EP3) exposure to different environments in a membrane protein. (**b**) schematic representation of a protein attached with the HO-1944 cross-linked nitroxide spin label which transforms into a simple pseudoatom (EPX) representation. EPX is covalently attached to the backbone $C\alpha_i$ and $C\alpha_{i+3}$ (or $C\alpha_{i+4}$). (**c**) The ten EPX-EPX distance restraints used for restrained molecular dynamics calculation. (**d**) During the RMD run, distance and accessibility (PaDSAR method) restraints were imposed. (**e**) Superimposition of crystal structure (PDB 1ORS) (yellow) and the simulated Up state model (blue). (**f**) Top: the best ten structures of Down state (red) models was superimposed with Up state model (blue). Bottom:

structure comparison between the two average models representing the up (blue) and down (red) conformations.

Cysteine mutant	Distance (Å)											
	x-ray	PCPG	U1	U2	U3	U4	U5	U6	U7	U8	U9	U10
39/43-118/121	33.1	28.6	27.6	27.7	27.5	27.8	27.6	27.6	27.7	27.5	27.5	27.7
39/43-121/125	28.8	20.9	21.9	22.3	21.7	22.0	21.8	21.9	21.9	21.9	21.8	21.8
40/44-118/121	38.1	33.7	35.2	35.5	35.2	35.3	35.5	35.4	35.5	35.2	35.3	35.5
40/44-121/125	33.6	29.6	30.2	30.9	30.2	30.3	30.5	30.5	30.6	30.4	30.4	30.5
57/61-118/121	38.3	34.9	35.8	35.6	35.4	35.6	35.4	35.6	35.6	35.1	35.7	35.5
57/61-121/125	33.9	33.8	32.6	32.6	32.5	32.5	32.5	32.6	32.6	32.5	32.6	32.6
72/75-118/121	38.1	38.1	39.1	39.1	38.7	39.0	38.8	38.8	38.8	38.7	38.6	38.9
72/75-121/125	32.4	33.1	34.3	34.5	34.4	34.3	34.5	34.2	34.3	34.3	34.1	34.1
74/77-118/121	22.2	26.4	27.4	27.4	27.2	27.3	27.2	27.3	27.0	27.2	27.2	27.3
74/77-121/125	16.9	24.5	23.5	23.5	23.7	23.5	23.7	23.5	23.5	23.7	23.5	23.6

Supplementary Table 1 EPX-EPX distances from the best ten structures (denoted as U1, U2, …, U10) compared with distances from the crystal structure and experimental PCPG data.

Cysteine mutant	Distance (Å)										
	DoTAP	D1	D2	D3	D4	D5	D6	D7	D8	D9	D10
39/43-118/121	30.8	29.8	29.8	29.9	29.8	29.8	29.9	29.8	29.8	29.8	29.8
39/43-121/125	23.6	24.6	24.4	24.6	24.5	24.4	24.6	24.5	24.5	24.5	24.7
40/44-118/121	34.2	34.6	34.7	34.7	34.6	34.9	35.0	34.5	34.6	34.6	34.5
40/44-121/125	29.1	30.1	30.0	30.2	30.0	30.0	30.5	30.0	30.0	30.1	30.1
57/61-118/121	36.8	36.1	36.0	36.2	36.3	36.4	36.0	36.2	35.9	36.0	36.1
57/61-121/125	33.4	32.4	32.4	32.4	32.4	32.4	32.4	32.4	32.4	32.3	32.4
72/75-118/121	36.1	37.9	37.9	37.8	37.4	38.5	37.4	37.8	37.5	37.6	38.1
72/75-121/125	32.1	32.9	32.8	32.6	32.3	33.0	32.6	32.7	32.7	32.6	33.0
74/77-118/121	26.9	26.8	27.0	27.1	26.8	27.5	26.6	27.0	26.6	26.7	27.0
74/77-121/125	24.1	23.2	23.3	23.3	23.3	23.2	23.4	23.3	23.1	23.1	23.2

Supplementary Table 2 EPX-EPX distances from the best ten structures (denoted as D1, D2, …, D10) compared with distances from experimental DoTAP data.